

Atomistic simulation of shear localization in Cu–Zr bulk metallic glass

Shigenobu Ogata^{a,b,c,*}, Futoshi Shimizu^{d,e}, Ju Li^d, Masato Wakeda^b, Yoji Shibutani^{a,b}

^a Center for Atomic and Molecular Technologies, Osaka University, Osaka 565-0871, Japan

^b Department of Mechanical Engineering, Osaka University, Osaka 565-0871, Japan

^c Handai Frontier Research Center, Osaka University, Osaka 565-0871, Japan

^d Department of Materials Science and Engineering, Ohio State University, Columbus, OH 43210, USA

^e Center for Computational Science and E-systems, Japan Atomic Energy Agency, Tokyo 110-0015, Japan

Available online 28 February 2006

Abstract

Shear deformations of Cu₅₇Zr₄₃ bulk metallic glass (BMG) model systems are performed using molecular dynamics simulation. The results suggest that both the hydrostatic stress and the stress normal to the shear plane should affect the shear response (modified Mohr–Coulomb yield criterion). We see shear localization and shear band nucleation in both a small system of 2000 atoms, and large systems of 524,288 atoms, and analyze local atomic structure evolution.

© 2006 Elsevier Ltd. All rights reserved.

Keywords: B. Glasses, metallic; B. Plastic deformation mechanisms; B. Yield stress; D. Defects: planar faults

1. Introduction

Computational investigations of the shear deformation response of bulk metallic glasses (BMG) [1–6] provide unique insights that complement experiments such as uniaxial tension/compression tests [7–10] and instrumented indentation [11–16]. There are two important factors, which may influence the shear response of BMGs. One is the nature of interatomic bonding. The shear deformation necessarily involves large bond angle changes and even neighbor swaps. Therefore the resistance to bond-angle change needs to be taken into account in more refined models, especially for BMGs having atomic types which tend to have directional bonding. For example, aluminum usually generates a directional bonding with surrounding atoms because of its bond covalency [17]. Thus BMGs having aluminum atoms may have stiff local atomic structures surrounding the aluminum atoms against shear deformation. Another important factor is short- and medium-ranged ordering [18], and its evolution under shear deformation, which should have strong strain-rate and temperature dependence.

In this initial investigation, we focus on the shear response of binary Cu–Zr BMG model system under quasi-static loading

and 0 K because results under the extremely lower strain rate and temperature can be useful reference for our future work at finite strain rate and temperature. Since it does not appear to have strong bond directionality, we can investigate this system using simple two-body potential within reasonable accuracy. There are many atomistic modeling studies of this system [1,2,19,20]. We have observed microscopic and mesoscopic structural evolutions, such as the nucleation of local shear transformation zone (STZ) and shear band, under volume-conserving simple shear deformation in molecular dynamics simulations based on Lennard–Jones 4–8 (L–J) potential [19]. We find that the shear deformation induces not only normal stress perpendicular to the shearing plane but also transverse normal stresses in the shearing plane, which suggests that the modified Mohr–Coulomb criterion [21] may be applicable.

2. Method

Cu₅₇Zr₄₃ BMG structures are generated using the melt quench procedure. We use parameters in Ref. [19] for the L–J potential. We first arrange the atoms randomly in a supercell, where periodic boundary condition (PBC) is applied in all three dimensions, and then heat it up to above the melting temperature. After staying at 1000 K for 0.1 ns, we cool it down to 0 K by rapid quench of cooling rate 10¹² K/s. The T_g is estimated as 1100 K. The supercell dimension is varied to maintain zero stress condition during the heating and cooling process. We cannot see any phase separations in the cooling process. To identify supercell size effect, we adopt three

* Corresponding author. Address: Center for Atomic and Molecular Technologies, Osaka University, Osaka 565-0871, Japan.

E-mail address: ogata@mech.eng.osaka-u.ac.jp (S. Ogata).

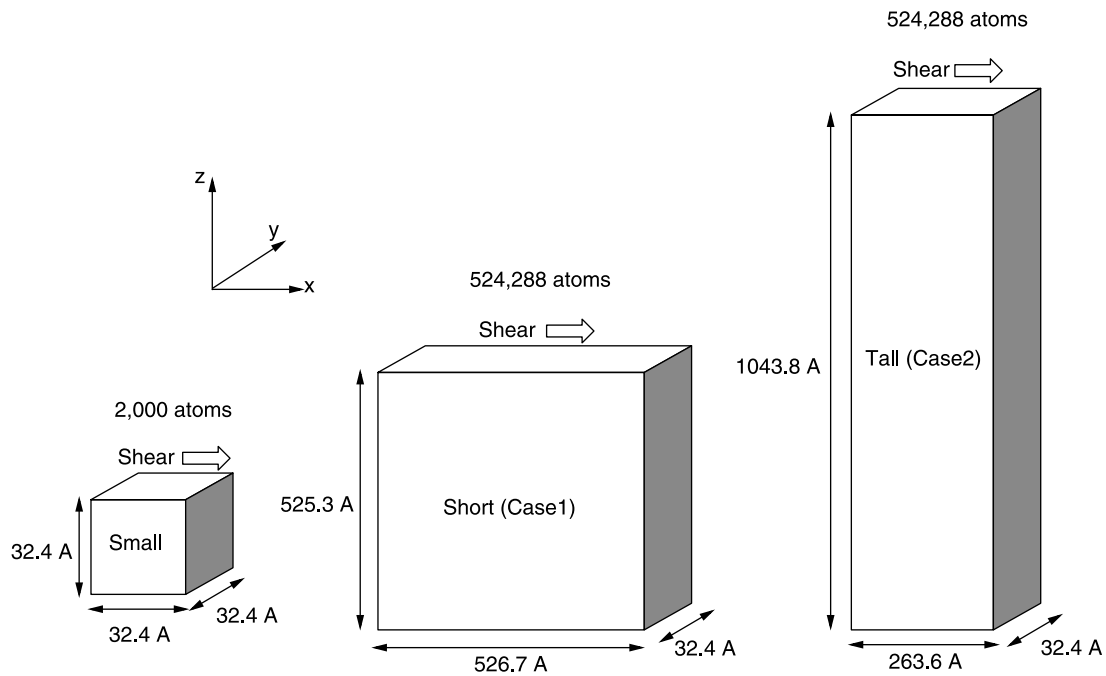


Fig. 1. Three different model sizes for shear deformation simulations.

different model sizes and shapes as illustrated in Fig. 1: a small test cell of 2000 atoms, and ‘full-sized’ cells of 524,288 atoms of two aspect ratios, short (Case 1) and tall (Case 2). We apply simple affine shear deformation to these cells by changing the supercell basis vectors directly, according to a prescribed

engineering shear strain schedule $\gamma(t)$. Actually we change only h_{31} component in \mathbf{H} matrix of the cell. The \mathbf{H} is defined in Section 3. A stepwise increment of engineering shear strain of $\Delta\gamma=0.1\%$ is used, and we relax the atomic configurations at each strain step by the steepest descent method.

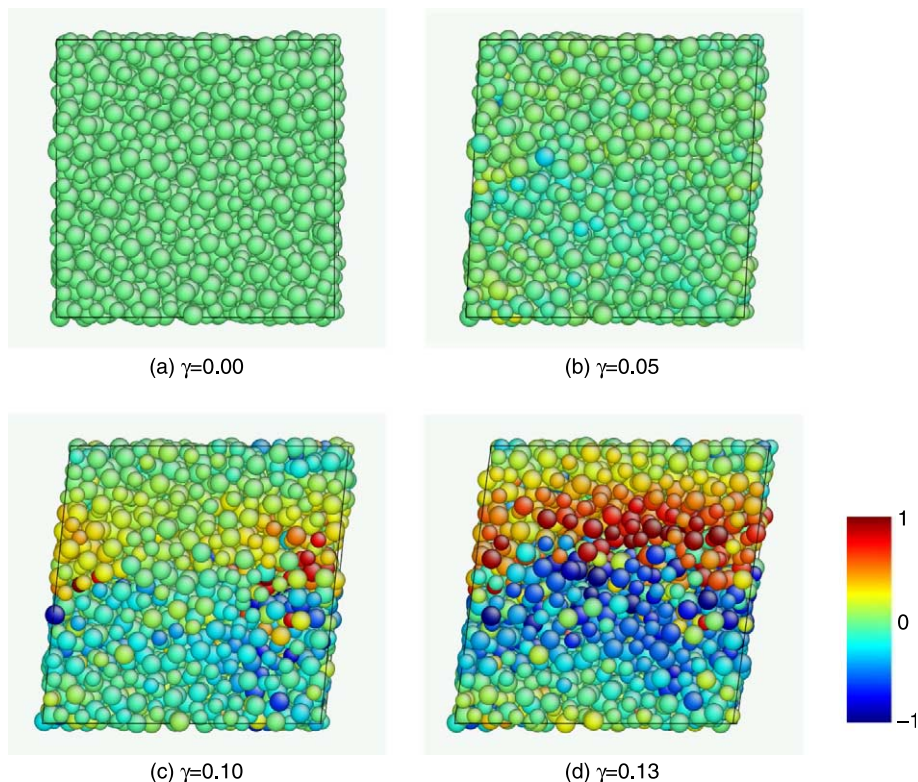


Fig. 2. Atomic configuration snapshots of the small supercell model under shear deformation. Each atom encodes inelastic displacement in the x -direction (in \AA). See details in the text.

3. Results

Figs. 2 and 3 show the evolutions of the atomic structure and stresses of the small supercell model with engineering shear strain γ . To quantify plastic deformation at the atomic level, we define the *inelastic displacement* of each atom i by the following equation

$$\mathbf{d}_i \equiv (\mathbf{x}_i \mathbf{H}^{-1} - \mathbf{x}_i^0 (\mathbf{H}^0)^{-1}) \mathbf{H}, \quad (1)$$

where \mathbf{x}_i is a 1×3 row-vector denoting the position of atom i , and \mathbf{H} is the 3×3 supercell matrix defined as

$$\mathbf{H} = \begin{pmatrix} \mathbf{h}_1 \\ \mathbf{h}_2 \\ \mathbf{h}_3 \end{pmatrix} = \begin{pmatrix} h_{11} & h_{12} & h_{13} \\ h_{21} & h_{22} & h_{23} \\ h_{31} & h_{32} & h_{33} \end{pmatrix}. \quad (2)$$

\mathbf{h}_1 , \mathbf{h}_2 and \mathbf{h}_3 are the supercell basis (row-) vectors. Superscript 0 denotes values at $\gamma = 0$. If the atoms move in an affine fashion following the supercell deformation without plastic relaxations, then (1) should be identically zero. Therefore \mathbf{d}_i and especially its x -component quantifies the amount of local inelastic relaxation, which color-encodes Fig. 2.

Before the shear stress σ_{13} reaches its maximum, we see STZ-like local atomic structure rearrangements at 7–11% engineering strain, because the shear deformation induces local instabilities. Correspondingly a few small shear stress drops can be found in the stress–strain curve. The whole system, however, is still staying in a globally mechanically stable condition. At 12% engineering strain, we observe a global atomic structure change due to an instability that percolates through the whole cell, resulting in the localization of inelastic shear strain in a narrow band. Shear sliding is found to occur mainly by breaking Cu–Cu bonds. Cascading stress drops with global downward trend can be found in the stress–strain curve after 12% engineering strain.

The nature of the global percolating instability is analyzed to be the following. When a local atomic rearrangement takes place, the elastic strain energy is released locally by generating local inelastic shear displacement in the shearing plane. This local

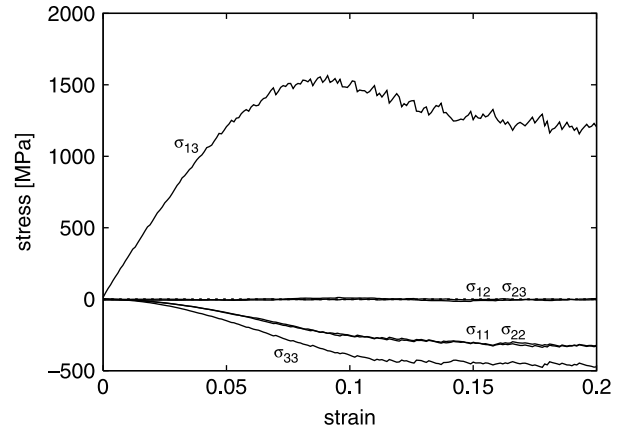


Fig. 4. Stress–strain curves of the short supercell model (Case 1) under shear deformation.

inelastic shear displacement, however, enhances the elastic strain energy of the surrounding materials in the in-plane directions. We define ‘hoop materials’ as the surrounding materials in the in-plane directions of a local region in which local shear transformation have taken place. If the hoop materials are already near a condition of elastic instability, a new local atomic rearrangement may take place. This may form a chain process that eventually organizes the shear band. At the same time this in-plane inelastic shear displacement will reduce the possibility of elastic instability in adjacent planes, by relieving the elastic strain energy of regions above and below the sliding plane. Therefore the shear band is usually sharply localized on a plane [22]. This discussion is similar in spirit to that of dislocation nucleation in crystalline solids [23]. It is suggested that the dislocation concept may be applicable to BMGs with modifications such as taking into account the structural features of BMGs instead of the Burgers vector concept in crystals.

The small supercell constrains the atomic configurations considerably, for example it does not nucleate more than one shear band. From Fig. 3, the shear deformation is seen to induce hydrostatic stress ($\sigma_{11} \approx \sigma_{22} \approx \sigma_{33}$ at large γ). But then because the data is noisy due to limited statistical sampling, we should confirm this by using larger supercell. Thus we perform the same

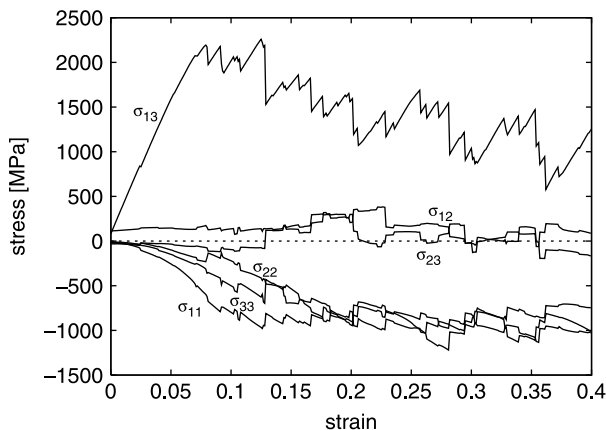


Fig. 3. Stress–strain curves of the small supercell model under shear deformation.

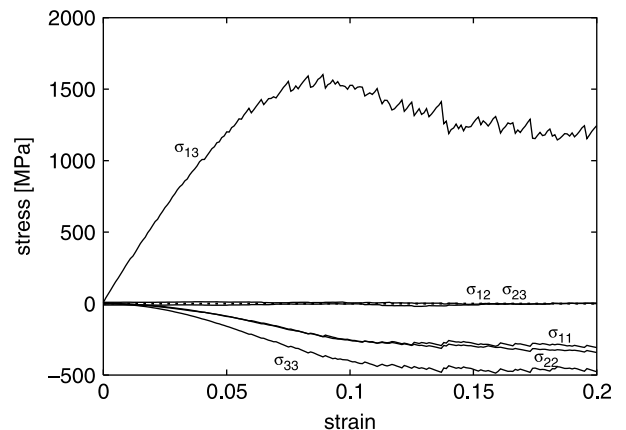


Fig. 5. Stress–strain curves of the tall supercell model (Case 2) under shear deformation.

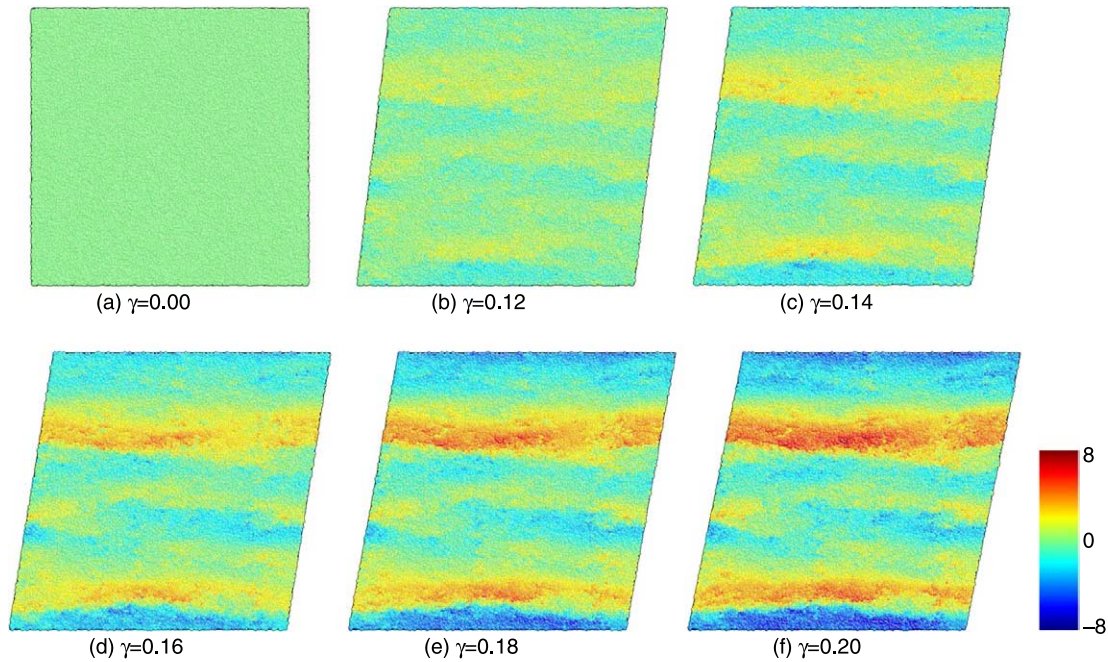


Fig. 6. Atomic configuration snapshots of the short supercell model (Case 1) under shear deformation. Each atom encodes inelastic displacement in the x -direction (in Å).

shear tests using the two large supercells with different aspect ratios, say short (Case 1) and tall (Case 2) models (Fig. 1).

Figs. 4 and 5 show stress–strain curves of the two shear tests. We get very smooth curves both for the short and tall models, and the two are very similar. The shear modulus and strength are estimated to be ~ 27 and ~ 1.5 GPa, respectively. Up to 2% shear strain, the shear stress σ_{13} shows linear dependence on the shear strain, and no shear strain–normal stress coupling can be found as ordained by the isotropic linear elastic constant $C_{ijkl} = \lambda\delta_{ij} + \mu(\delta_{ik}\delta_{jl} + \delta_{il}\delta_{jk})$. At greater than 2% shear strain, the nonlinear response of $\sigma_{13}(\gamma)$ starts to manifest. At the same time, shear strain–normal stress coupling is found. The nonlinear $\sigma_{13}(\gamma)$ response is not only due to the elastic nonlinearity related to interatomic interactions, but also the local inelastic atomic structural rearrangements, as a couple of small stress discontinuities are seen on the stress–strain curves. The shear deformation induces the normal stress σ_{33} ,

which is perpendicular to the shearing plane x – y , and normal stresses σ_{11} and σ_{22} , which are in the shearing plane. σ_{11} is always equal to σ_{22} , and above 2% strain σ_{33} is always a bit more negative than σ_{11} and σ_{22} . This special behavior of σ_{33} cannot be clearly seen in the small model.

Generally we find reciprocity in material responses: if a normal stress is affected by the shear strain, then the shear response will be affected by the normal strain. The above simulation results suggest that not only the normal stress to the sliding plane, but also the hydrostatic stress will significantly affect the shear stress response σ_{13} . The maxima of normal stresses σ_{11} , σ_{22} and σ_{33} of the large models are more than two times lower than that for the previous small model, due to elimination of statistical sample fluctuation. This shows that care is needed to determine model size and ensemble averaging procedure, otherwise we may get noisy results. We believe that the characteristic shear–normal stress coupling cannot be

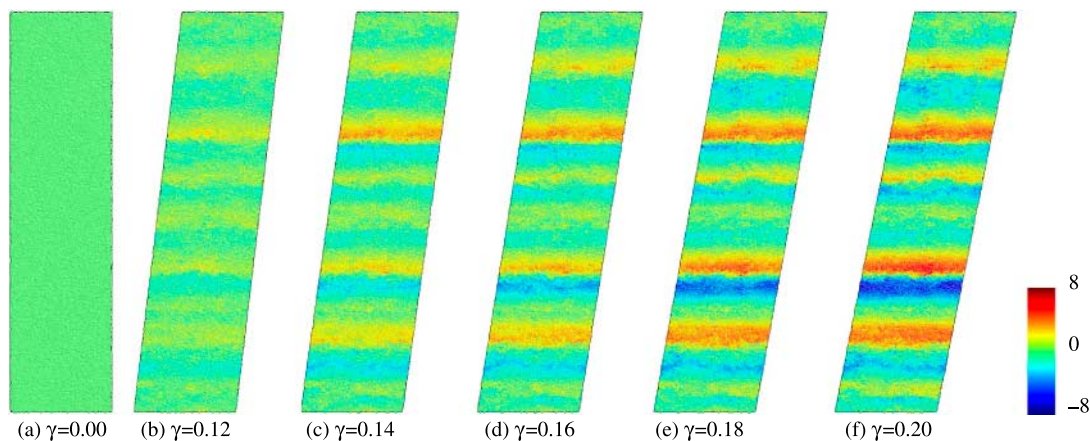


Fig. 7. Atomic configuration snapshots of the tall supercell model (Case 2) under shear deformation. Each atom encodes inelastic displacement in the x -direction (in Å).

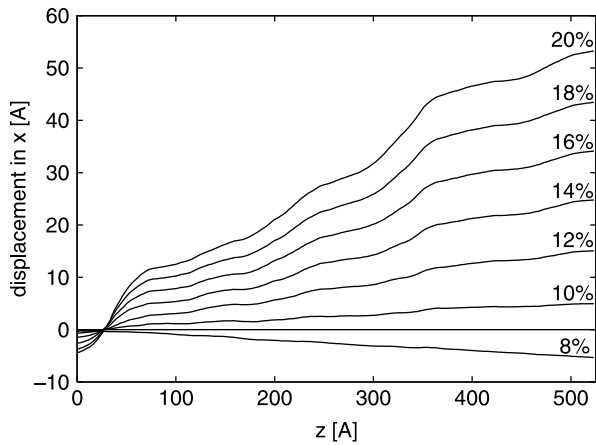


Fig. 8. Average atomic displacements in the x -direction in reference to 9% affine strain in the short supercell model (Case 1).

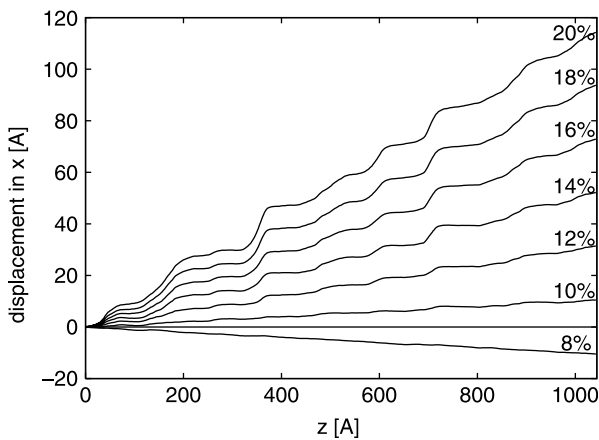


Fig. 9. Average atomic displacements in the x -direction in reference to 9% affine strain in the tall supercell model (Case 2).

ignored when we discuss the mechanical behaviors of BMGs. Thus for the yield criterion of BMG, both stress normal to slip plane and hydrostatic stress should be taken into account, which suggests the modified Mohr–Coulomb yield criterion [21] is possibly applicable to BMGs. Some experimental data show the hydrostatic stress independence for the yield criterion [8,9]. This discrepancy may occur because of the difference in composition under consideration. If a BMG has elements like Al, Ni, and O impurities, which cannot be treated by two-body potentials, a different mechanism may operate during the shear deformation.

Figs. 6 and 7 show the inelastic displacement of each atom in x for the two large models. Figs. 8 and 9 plot the average atomic displacement in x in reference to 9% affine strain, averaged over different z -slices. Both for the short and tall supercells, severe shear localizations are seen at strains larger than 8%. The localization is initiated at different z positions

almost simultaneously. Once the shear localization takes place at a z position, the z position does not change in the ensuing strain steps. Above 15% strain, the stress–strain curves become flat because all the additional work is dispensed in the sliding the shear bands.

4. Conclusions

Using atomistic simulation with a binary L–J 4–8 potential, simple shear deformations are performed on $\text{Cu}_{57}\text{Zr}_{43}$ bulk metallic glass (BMG) model system. We demonstrate shear strain localization and shear band nucleation, and discuss the localization mechanism. We find significant shear–normal stress coupling which suggests the modified Mohr–Coulomb yield criterion.

Acknowledgements

S.O. and Y.S. acknowledge support by the Ministry of Education, Science, Sports and Culture, Grant-in-Aid for Scientific Research on Priority Areas, 428-15074214, 2005. J.L. acknowledges support by Honda R&D Co., Ltd., NSF, AFOSR, ONR and the Ohio Supercomputer Center.

References

- [1] Lund AC, Schuh CA. *Intermetallics* 2004;12:1159.
- [2] Schuh CA, Lund AC. *Nature Mater* 2003;2:449.
- [3] Varnik F, Bocquet L, Barrat JL, Berthier L. *Phys Rev Lett* 2003;90:095701.
- [4] Varnik F, Bocquet L, Barrat JL. *J Chem Phys* 2004;120:2788.
- [5] Fu XY, Falk ML, Rigney DA. *Wear* 2001;250:420.
- [6] Fu XY, Rigney DA, Falk ML. *J Non-Cryst Solids* 2003;317:206.
- [7] Mukai T, Nieh TG, Kawamura Y, Inoue A, Higashi K. *Intermetallics* 2002;10:1071.
- [8] Lowhaphandu P, Montgomery SL, Lewandowski JJ. *Scripta Mater* 1999;41:19.
- [9] Lewandowski JJ, Lowhaphandu P. *Philos Mag A* 2002;82:3427.
- [10] Yang B, Morrison ML, Liaw PK, Buchanan RA, Wang GY, Liu CT, Denda M. *Appl Phys Lett* 2005;86:141904.
- [11] Argon AS. *Acta Metall* 1979;27:47.
- [12] Bei H, Lu ZP, George EP. *Phys Rev Lett* 2004;93:125504.
- [13] Kim JJ, Choi Y, Suresh S, Argon AS. *Science* 2002;295:654.
- [14] Schuh CA, Nieh TG. *Acta Mater* 2003;51:87.
- [15] Tang C, Li Y, Zeng K. *Mater Sci Eng A* 2004;384:215.
- [16] Vaidyanathan R, Dao M, Ravichandran G, Suresh S. *Acta Mater* 2001;49:3781.
- [17] Ogata S, Li J, Yip S. *Science* 2002;298:807.
- [18] Miracle DB. *Nature Mater* 2004;3:697.
- [19] Kobayashi S, Maeda K, Takeuchi S. *J Phys Soc Jpn* 1980;48:1147.
- [20] Lund AC, Schuh CA. *Acta Mater* 2003;51:5399.
- [21] Donovan PE. *Acta Metall* 1989;37:445.
- [22] Sergueeva AV, Mara NA, Kuntz JD, Branagan DJ, Mukherjee AK. *Mater Sci Eng A* 2004;383:219.
- [23] Li J, Ngan AHW, Gumbsch P. *Acta Mater* 2003;51:5711.